Electronic Supplementary Material (ESI) for Nanoscale Advances.

High-performance flower-like and biocompatible nickel-coated Fe_3O_4@SiO_2 magnetic nanoparticles decorated on graphene electrocatalyst for oxygen evolution reaction

Li Ye, [a] Pengcheng Zhu, [a] Tianxing Wang, [a] Xiaolei Li, [b] and Lin Zhuang *[a]

[a] School of Physics, Institute for Solar Energy Systems, Guangdong Provincial Key Laboratory of Photovoltaics Technologies, Sun Yat-sen University, Guangzhou 510006, China

[b] Fels Cancer Institute of Personalized Medicine and Department of Cancer and Cellular Biology, Lewis Katz School of Medicine, Temple University, Philadelphia, PA, USA

*stszhl@mail.sysu.edu.cn

Table S1. Comparisons of OER performance over Fe/Ni-based catalysts in alkaline medium.

Catalyst	WE[a)]	Electrolyte [M KOH]	J[b)]	η[c)]	TS[d)]	Ref.
N-MCF/N-MGF(Fe_3O_4)	GC	0.1	10	324	67	[1]
$MnFe_2O_4$/Ni Foam	GC	1	10	310	65	[2]
Fe_3O_4@Co_9S_8/rGO-2	GC	1	10	320	54.5	[3]
g-C_3N_4/CeO_2/Fe_3O_4	GC	1	10	310	51	[4]
Fe_3O_4/Ni-BDC	GC	1	10	295	47.8	[5]
Fe_3O_4-CoP_x/TiN	GC	1	10	331	122	[6]
Ni_2P	GC	1	10	320	105	[7]
Ni_3Fe@Fe_3O_4/$NC_{10\%}$	GC	1	10	350	56	[8]
Co_3O_4 nanosheet	GC	1	10	384	52	[9]
$SrCo_{0.8}Fe_{0.5-x}O_{3-\delta}$/$Fe_xO_y$	GC	1	10	350	79	[10]
Fe_3O_4@NiSx/rGO	GC	1	10	330	35.5	[11]
Co_3O_4/Fe_3O_4	GC	0.1	10	410	62	[12]
H-Co_9S_8/ Fe_3O_4@SNC	GC	0.1	10	280	87	[13]
Ni_3B	GC	1	10	302	52	[14]
Pt/NiO	GC	1	10	358	33	[15]
$Ni_{2-x}Fe_xO$	GC	0.5	10	325	53	[16]
NiO_x/P-CNTs	GC	0.1	10	350	40	[17]
Ni-O-Ni	GC	1	10	300	74	[18]
Ni_3Se_2	GC	1	10	310	97.1	[19]
N-NiO	GC	0.1	10	400	56	[20]
NiO-NPs	GC	1	10	481	238	[21]
Ni_3FeN/r-GO	GC	1	10	270	94	[22]
NiO/Ni-Fe LDH	GC	1	10	270	30	[23]
$NiCo_2P_x$/CNTS	GC	1	10	284	50.3	[24]
NiO/MnO_2	GC	0.1	10	345	42	[25]

Ni_3N	GC	1	10	290	45	[26]
$Co_{2.25}Fe_{0.75}O_4$	GC	1	10	350	50	[27]
Ni-MOF	GC	1	10	280	64	[28]
R-Fe_3O_4	GC	1	10	320	61.47	[29]
Ni/Fe_3O_4@ONC	GC	1	10	296	61	[30]
Fe_3O_4@SiO_2@NiO/Graphene/C_3N_4	GC	1	10	288	40.46	This work

[a)] WE are the working electrode (GC, Glass carbon); [b)] J is current density (mA cm^{-2}); [c)] η is overpotential (mV); [d)] TS is Tafel slope (mV dec^{-1}).

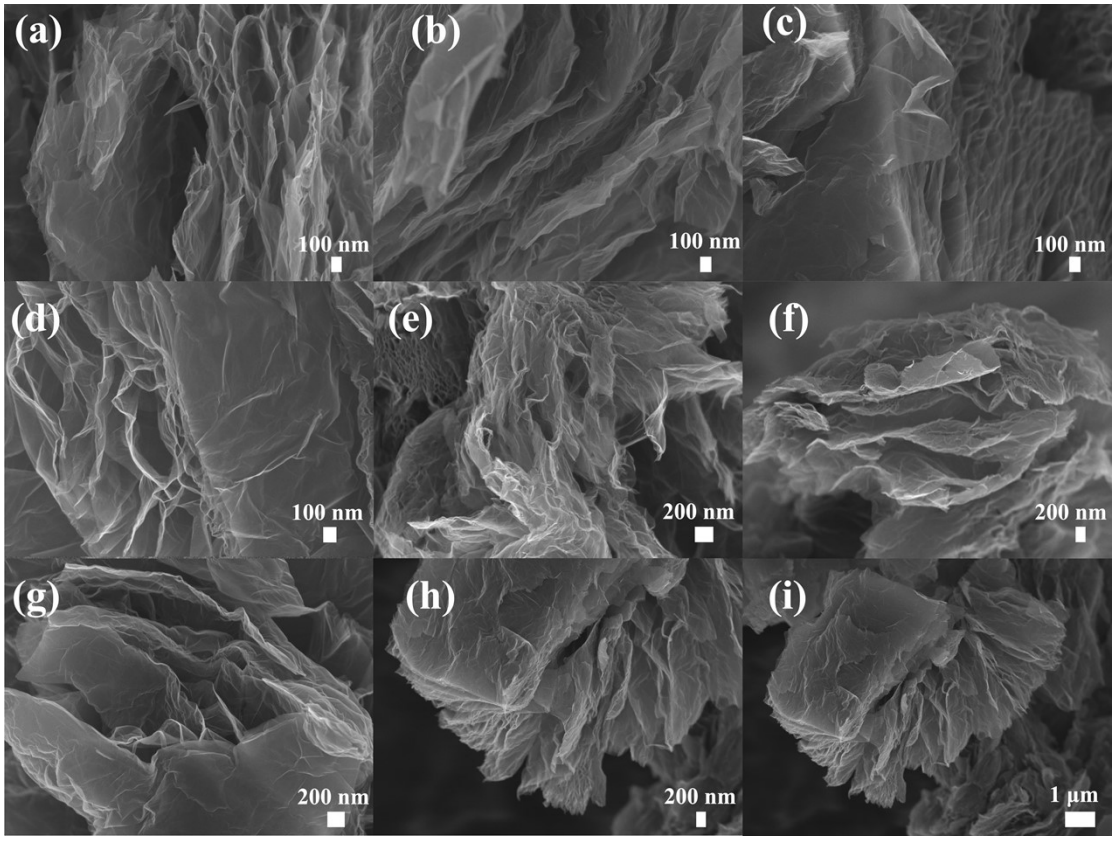

Fig. S1. (a)-(i) SEM images of graphene.

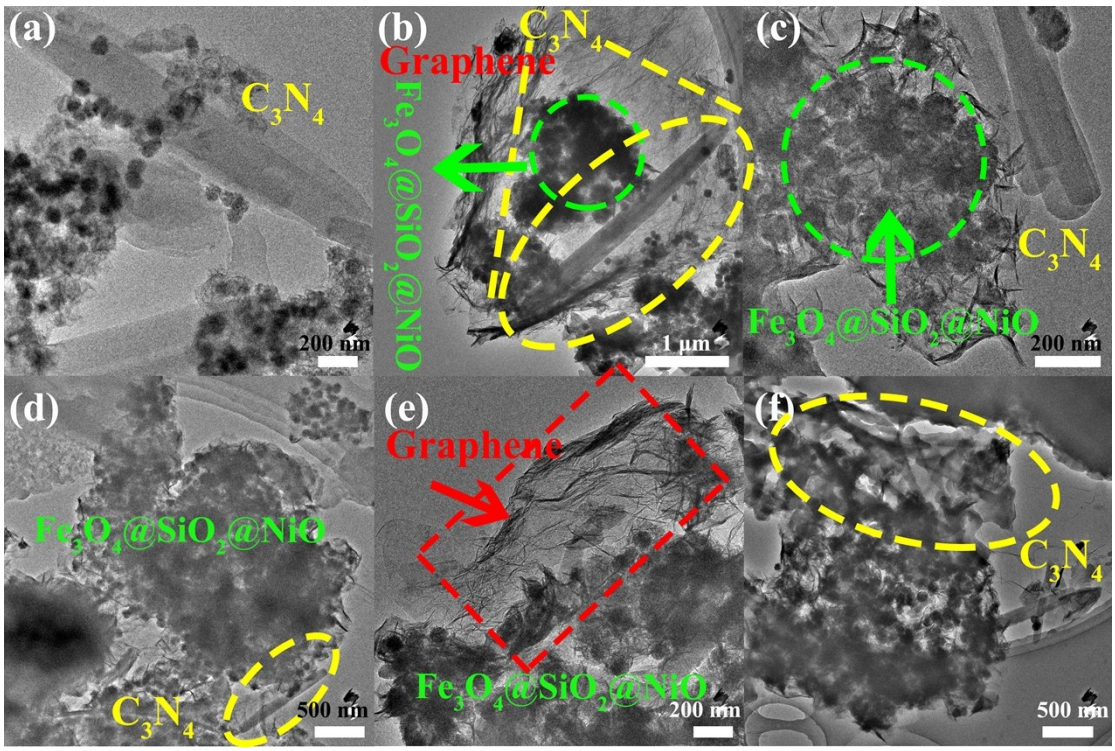

Fig. S2. (a)-(f) TEM image of $Fe_3O_4@SiO_2@NiO/Graphene/C_3N_4$.

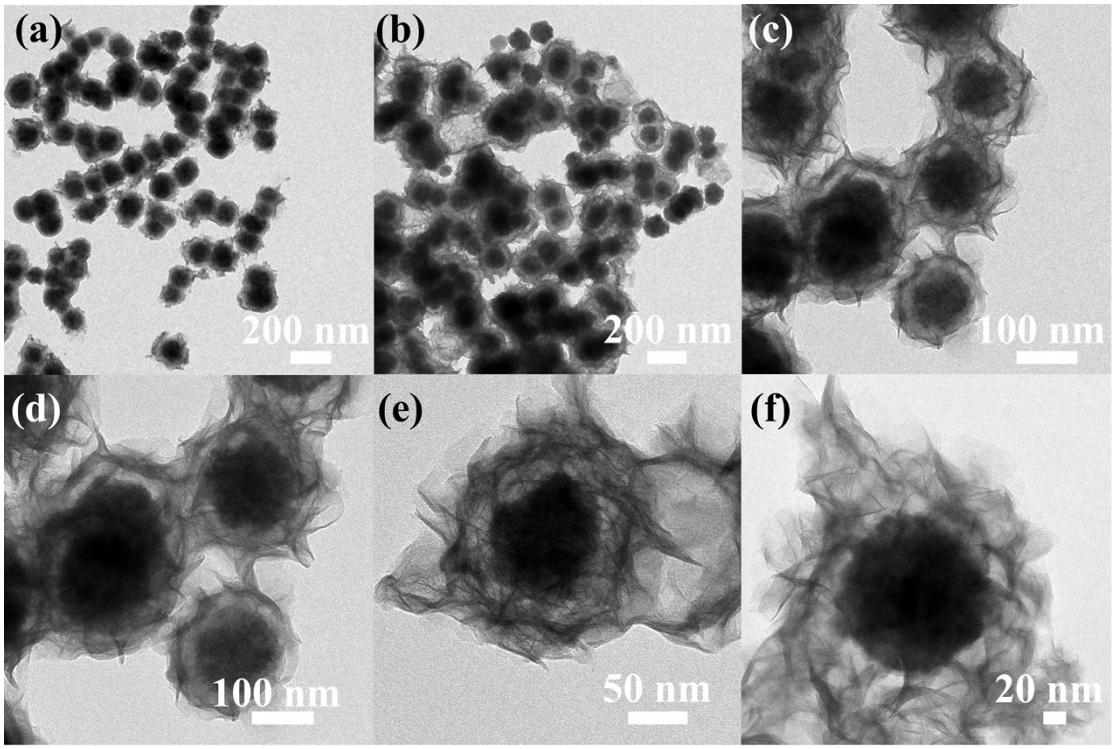

Fig. S3. (a)-(f) TEM image of $Fe_3O_4@SiO_2@NiO$.

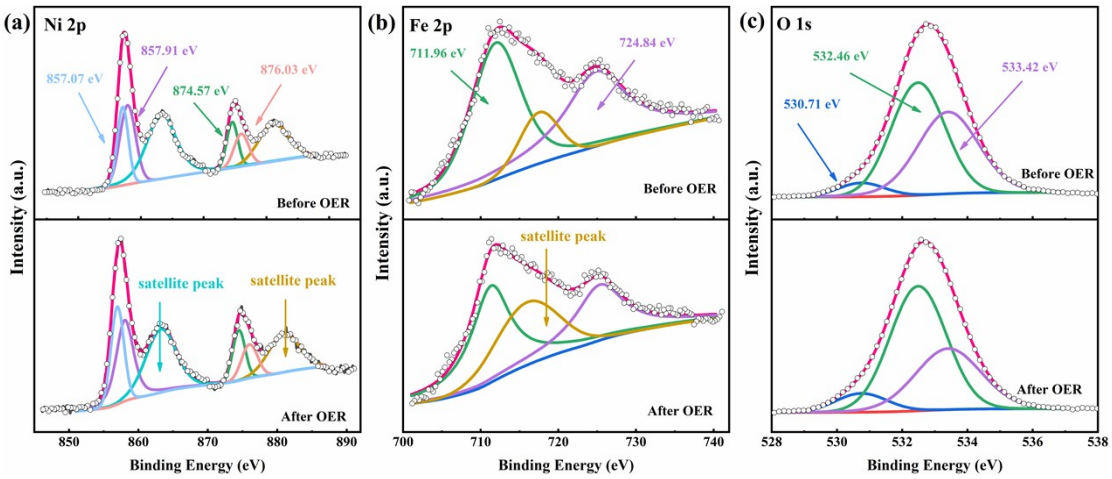

Fig. S4. The Ni 2p (a), Fe 2p (b), and O 1s (c) XPS spectra results of Fe_3O_4@SiO_2@NiO/Graphene/C_3N_4 before and after OER.

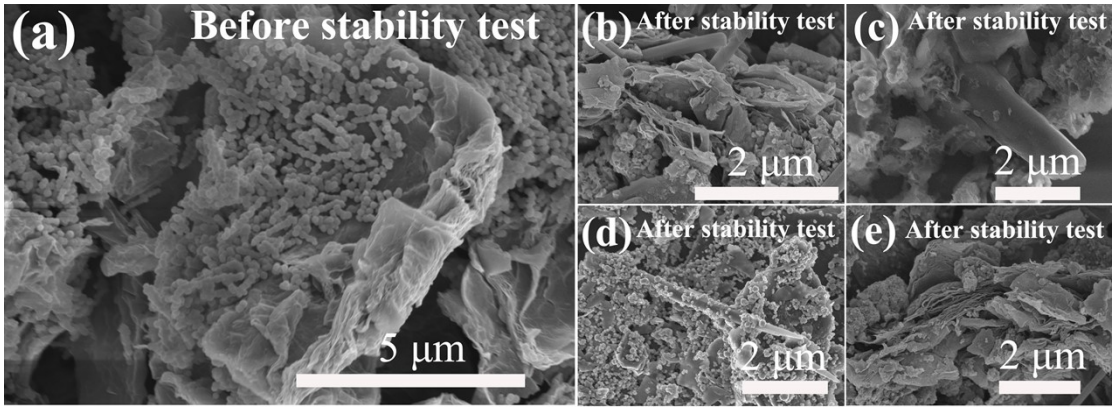

Fig. S5. SEM images of Fe_3O_4@SiO_2@NiO/Graphene/C_3N_4 catalyst before (a) and after (b-e) stability test.

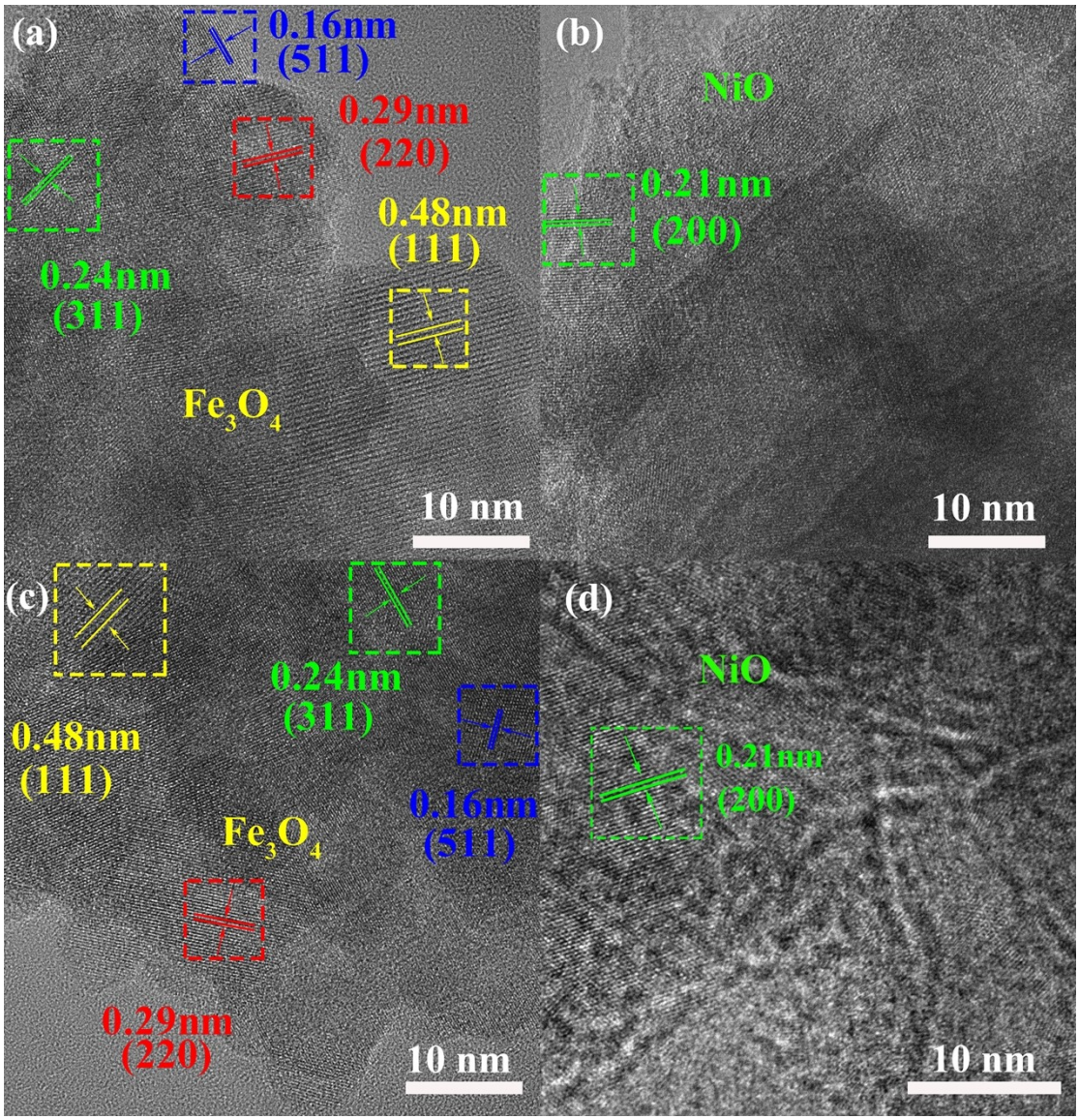

Fig. S6. HRTEM images of Fe_3O_4@SiO_2@NiO/Graphene/C_3N_4 catalyst before (a, b) and after OER (c, d).

Section1. Discussion of Mechanism of OER

OER kinetics are a multi-electron charge transfer process in alkaline medium and we consider a four-electron reaction mechanism for OER. Under alkaline conditions, the water oxidation reaction is given by (equation (1)):

$$4OH^- \rightarrow O_2(g) + 2H_2O + 4e^- \qquad \text{* MERGEFORMAT (1)}$$

The OER reaction also includes the adsorption of reactive species on the electrode surface, the transfer of electrons, and the desorption process of reactive species. In general, this reaction is usually assumed to proceed in the following four elementary steps [31-33] and the OER mechanism in an alkaline electrolyte is depicted as follows (equations (2)-(5)):

$$* + OH^- \rightarrow *OH + e^- \qquad \text{* MERGEFORMAT (2)}$$

$$*OH + OH^- \rightarrow *O + H_2O + e^- \quad \text{* MERGEFORMAT (3)}$$

$$*O + OH^- \rightarrow *OOH + e^- \quad \text{* MERGEFORMAT (4)}$$

$$*OOH + OH^- \rightarrow * + O_2 + H_2O + e^- \quad \text{* MERGEFORMAT (5)}$$

where the * denotes the active site on the catalyst surface. The Tafel plots describe the kinetics and mechanism of OER. Based on the above mechanism, the free energy of three intermediate states, *OH, *O, and *OOH, are important to identify a given material's OER activity.

In general, the electrochemical reactions at the cathode and anode parts for the water-splitting reaction are different under alkaline conditions (equations (6) and (7)). The OER reaction involves four electron transfers, and the kinetics of the M-O bond fracture process is very slow. It has a high overpotential and consumes a high amount of energy in the anodic reaction of electrolytic water.

Alkaline conditions:

Cathode reaction:

$$4H_2O + 4e^- \rightarrow 2H_2 + 4OH^- \quad E_c^0 = -0.83V \quad \text{* MERGEFORMAT (6)}$$

Anode reaction:

$$4OH^- \rightarrow 2H_2 + 2H_2O + 4e^- \quad E_a^0 = -0.40V \quad \text{* MERGEFORMAT (7)}$$

Possible OER mechanisms in an alkaline medium have been proposed, as demonstrated in equations (8)-(12). It is worth noting that the diagram in Fig. S7 displays two different approaches to form O_2 from a produced MO intermediate in different electrolytes, where "M" also denotes the active site. As illustrated in the green route in Fig. S7, the first type is the direct combination of two M-O intermediates to produce O_2 (equation (10)). The other method is for M-O to first form a peroxide (M–OOH) intermediate (equations (11)) and subsequently decompose to O_2 (blue route in Fig. S7; equations (12)). Most of the proposed mechanisms involve MOH and MO intermediates [34-36]. During the heterogeneous OER process, all M–O bonding interactions within the intermediates (MOH, MO, and MOOH) are crucial to determining the overall electrocatalytic activity. Further, Fig. S8 displays a Schematic diagram of the three-electrode system and OER process in our experiments.

The proposed mechanism under alkaline conditions:

$$M + OH^- \rightarrow MOH + e^- \quad \text{* MERGEFORMAT (8)}$$

$$MOH + OH^- \rightarrow MO + H_2O + e^- \quad \text{* MERGEFORMAT (9)}$$

$$2MO \rightarrow 2M + O_2 \quad \text{* MERGEFORMAT (10)}$$

$$MO + OH^- \rightarrow MOOH + e^- \quad \text{* MERGEFORMAT (11)}$$

$$MOOH + OH^- \rightarrow M + O_2 + H_2O + e^- \ * \text{ MERGEFORMAT} \quad (12)$$

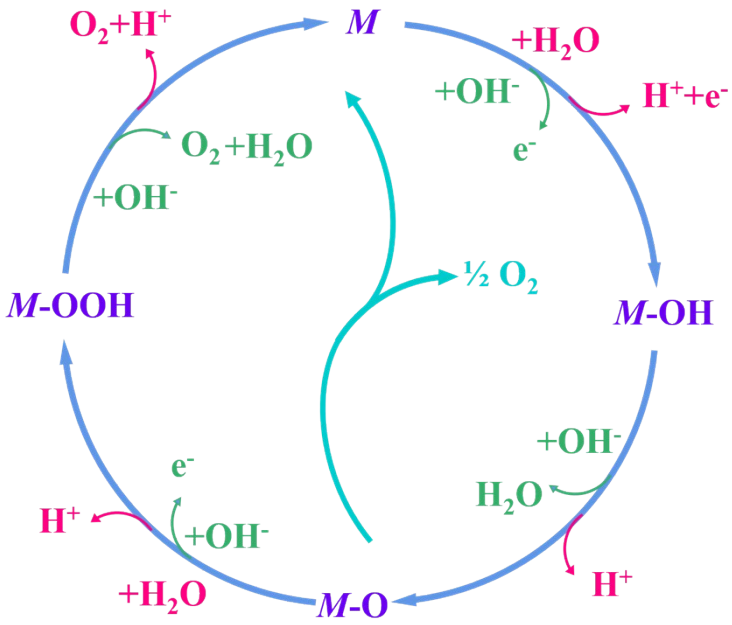

Fig. S7. The oxygen evolution reaction (OER) mechanism in acid (pink line) and alkaline (green line) medium. Two reaction routes of oxygen evolution take place: (1) the blue line indicates that the oxygen evolution involves the formation of a peroxide (M–OOH) intermediate (blue line); (2) while another route for the direct reaction of two adjacent oxos (M–O) intermediates (aqua green line) to produce molecular oxygen.

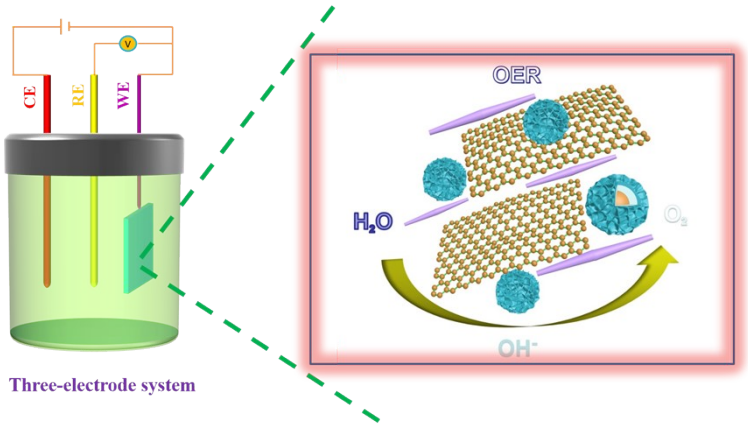

Fig. S8. Schematic diagram of the three-electrode system and OER.

Section2. Discussion of the structure-activity relationship between the catalyst and OER performance

As illustrated in Figs. S9 (a-f), the decoration of graphene can effectively improve the OER activity of the catalyst, and with the continuous addition of C_3N_4, the catalytic performance of Fe_3O_4@SiO_2@NiO/Gr/C_3N_4 will continues to enhance, ultimately

presenting the best catalytic performance. In sum, Fe_3O_4@SiO_2@NiO/Gr/C_3N_4 exhibits superior OER performance and long-term durability compared to other catalysts. The OER electrocatalytic performance increased with the addition of different components, and the details are explained as follows:

Firstly, the Fe_3O_4@SiO_2@NiO magnetic nanoparticles generated by the solvothermal method possess strong binding and low interfacial resistance between the two-dimensional structure of electrically conducting graphene and the Fe_3O_4@SiO_2@NiO magnetic nanoparticles are uniformly distributed on the surface of the graphene and its good contact with the graphene nanosheets also reduces the external transport resistance in electrocatalysis.

Secondly, the two-dimensional structure and large specific surface area (900 m^2/g) of graphene ensure more exposed active sites and more activated reactive molecules involved in catalytic reactions while accelerating mutual electron transport, and the carbon framework architecture also improves electron mobility and electrical conductivity, all of which improve our catalytic efficiency. The high specific surface area of C_3N_4 also increases the contact area, and the electron transfer rate is improved. The significantly improved electrocatalytic performance results from their large surface area, excellent internal diffusion property, and superior intrinsic conductivity.

Thirdly, one-dimensional rod-shaped C_3N_4 possesses a large specific surface area due to its outstanding aspect ratio, which accelerates the electron transfer rate faster and can exhibit more excellent electrocatalytic performance. The addition of C_3N_4 with a high specific surface area, on the one hand, increases the contact area, and the increase of active site in the electrocatalytic reaction reduces the OER reaction barrier [37]. On the other hand, it also improves conductivity and electron diffusion rate, increasing electron transfer rate and excellent OER electrocatalytic performance. The introduction of the N element greatly contributed to the performance of the oxygen evolution reaction of the catalyst [38-42]. The presence of repeating s-triazine units in the C_3N_4 structure can make it easier to coordinate with nanoparticles to form composites, and this strong coordination interaction helps electron transport. Moreover, C_3N_4 has good chemical stability and high pyridine nitrogen content, which helps to enhance the electrocatalytic performance, e.g.: ACS Appl Mater Interfaces **2018,** 10 (45), 39161-39167; ChemCatChem **2018,** 10 (24), 5587-5592; The Journal of Physical Chemistry C **2017,** 121 (36), 19548-19558; J Am Chem Soc **2017,** 139 (9), 3336-3339 [43-52].

Furthermore, the synergistic effect between different components in the composite ultimately improves the electrocatalytic efficiency of the obtained Fe_3O_4@SiO_2@NiO/Graphene/C_3N_4 catalyst. The addition of C_3N_4 and graphene with a high specific surface area can increase the contact area between the different materials, and significantly improve the conductivity of the overall system, thereby increasing the electron diffusion rate between the different materials. Besides, different components are connected through close contact to achieve interconnectivity and conductivity. The different components are in close contact with each other and build bridges to form the structure, resulting in increased interaction

between them. Benefiting from the synergistic effect between different components of the catalyst, the Fe_3O_4@SiO_2@NiO/Graphene/C_3N_4 catalyst exhibits highly active electrochemical OER in alkaline electrolytes. In conclusion, such a high catalytic reactivity is attributed to the synergic effect of multiple elements.

Therefore, the synergistic effect between different components finally effectively improves the catalyst's electrocatalytic efficiency [41-46]. This work provides a feasible approach to achieve the strong combination of carbon materials and metal oxides for excellent OER performance.

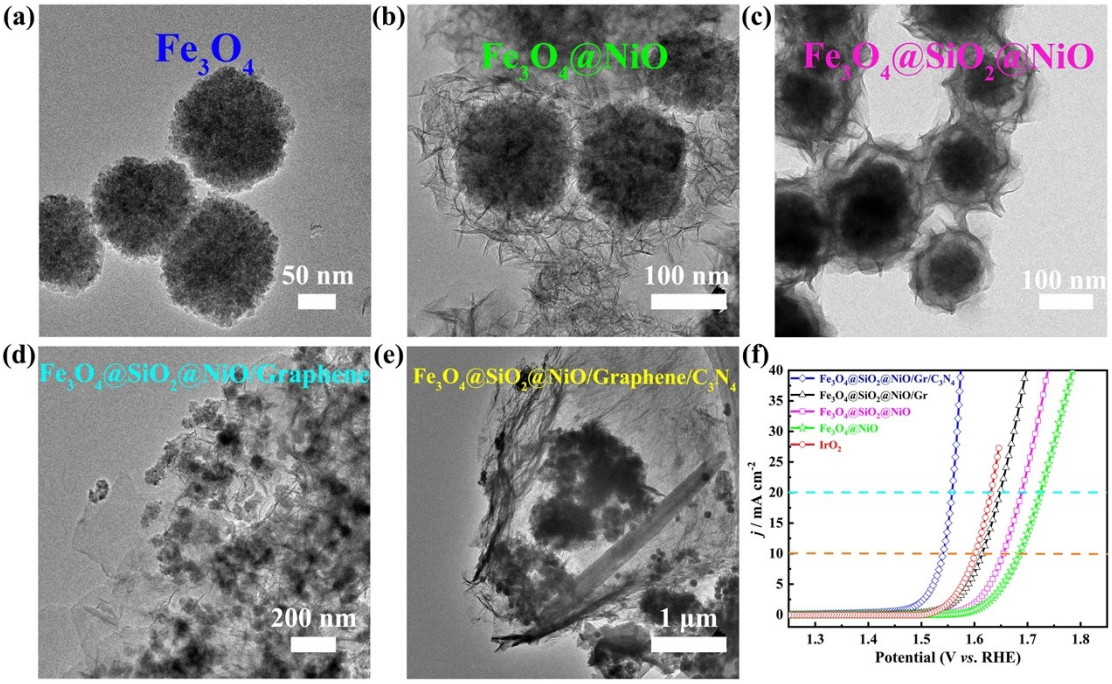

Fig. S9. TEM images of (a) Fe_3O_4, (b) Fe_3O_4@NiO, (c) Fe_3O_4@SiO_2@NiO, (d) Fe_3O_4@SiO_2@NiO/Graphene and (e) Fe_3O_4@SiO_2@NiO/Graphene/C_3N_4. (f) Corresponding LSV curves with different components.

References

[1] Zhang, C.; Wang, B.; Shen, X.; Liu, J.; Kong, X.; Chuang, S. S. C.; Yang, D.; Dong, A.; Peng, Z., A nitrogen-doped ordered mesoporous carbon/graphene framework as bifunctional electrocatalyst for oxygen reduction and evolution reactions. *Nano Energy* **2016,** *30*, 503-510.

[2] Kim, J.; Lee, J.; Liu, C.; Pandey, S.; Woo Joo, S.; Son, N.; Kang, M., Achieving a long-term stability by self-redox property between Fe and Mn ions in the iron-manganese spinel structured electrode in oxygen evolution reaction. *Applied Surface Science* **2021,** *546*.

[3] Yang, J.; Zhu, G.; Liu, Y.; Xia, J.; Ji, Z.; Shen, X.; Wu, S., Fe_3O_4-Decorated Co_9S_8 Nanoparticles In Situ Grown on Reduced Graphene Oxide: A New and Efficient Electrocatalyst for Oxygen Evolution Reaction. *Advanced Functional Materials* **2016,** *26* (26), 4712-4721.

[4] Rashid, J.; Parveen, N.; Haq, T. u.; Iqbal, A.; Talib, S. H.; Awan, S. U.; Hussain, N.; Zaheer, M., g-C_3N_4/CeO_2/Fe_3O_4 Ternary Composite as an Efficient Bifunctional Catalyst for Overall Water Splitting. *ChemCatChem* **2018,** *10* (24), 5587-5592.

[5] Huang, W.; Peng, C.; Tang, J.; Diao, F.; Nulati Yesibolati, M.; Sun, H.; Engelbrekt, C.; Zhang, J.; Xiao, X.; Mølhave, K. S., Electronic structure modulation with ultrafine Fe_3O_4 nanoparticles on 2D Ni-based metal-organic framework layers for enhanced oxygen evolution reaction. *Journal of*

Energy Chemistry **2022,** *65*, 78-88.
[6] Guo, B.; Sun, J.; Hu, X.; Wang, Y.; Sun, Y.; Hu, R.; Yu, L.; Zhao, H.; Zhu, J., Fe_3O_4-CoPx Nanoflowers Vertically Grown on TiN Nanoarrays as Efficient and Stable Electrocatalysts for Overall Water Splitting. *ACS Applied Nano Materials* **2018,** *2* (1), 40-47.
[7] Wang, T.; Liu, L.; Zhu, Z.; Papakonstantinou, P.; Hu, J.; Liu, H.; Li, M., Enhanced electrocatalytic activity for hydrogen evolution reaction from self-assembled monodispersed molybdenum sulfidenanoparticles on an Au electrode. *Energy Environ. Sci.* **2013,** *6* (2), 625-633.
[8] Gebreslase, G. A.; Sebastián, D.; Martínez-Huerta, M. V.; Lázaro, M. J., Nitrogen-doped carbon decorated-$Ni_3Fe@Fe_3O_4$ electrocatalyst with enhanced oxygen evolution reaction performance. *Journal of Electroanalytical Chemistry* **2022,** *925*.
[9] Elakkiya, R.; Maduraiveeran, G., Two-Dimensional Earth-Abundant Transition Metal Oxides Nanomaterials: Synthesis and Application in Electrochemical Oxygen Evolution Reaction. *Langmuir* **2020,** *36* (17), 4728-4736.
[10] Yi, Y.; Wu, Q.; Li, J.; Yao, W.; Cui, C., Phase-Segregated $SrCo_{0.8}Fe_{0.5-x}O_{3-\delta}/Fe_xO_y$ Heterostructured Catalyst Promotes Alkaline Oxygen Evolution Reaction. *ACS Appl Mater Interfaces* **2021,** *13* (15), 17439-17449.
[11] Zhu, G.; Xie, X.; Liu, Y.; Li, X.; Xu, K.; Shen, X.; Yao, Y.; Shah, S. A., Fe_3O_4@NiSx/rGO composites with amounts of heterointerfaces and enhanced electrocatalytic properties for oxygen evolution. *Applied Surface Science* **2018,** *442*, 256-263.
[12] Ng, K.-L.; Kok, K.-Y.; Ong, B.-H., Facile Synthesis of Self-Assembled Cobalt Oxide Supported on Iron Oxide as the Novel Electrocatalyst for Enhanced Electrochemical Water Electrolysis. *ACS Applied Nano Materials* **2017,** *1* (1), 401-409.
[13] Gan, L.; Fang, J.; Wang, M.; Hu, L.; Zhang, K.; Lai, Y.; Li, J., Preparation of double-shell Co_9S_8/Fe_3O_4 embedded in S/N co-decorated hollow carbon nanoellipsoid derived from Bi-Metal organic frameworks for oxygen evolution reaction. *Journal of Power Sources* **2018,** *391*, 59-66.
[14] Jiang, W. J.; Niu, S.; Tang, T.; Zhang, Q. H.; Liu, X. Z.; Zhang, Y.; Chen, Y. Y.; Li, J. H.; Gu, L.; Wan, L. J.; Hu, J. S., Crystallinity-Modulated Electrocatalytic Activity of a Nickel(II) Borate Thin Layer on Ni_3B for Efficient Water Oxidation. *Angew Chem Int Ed Engl* **2017,** *56* (23), 6572-6577.
[15] Lin, C.; Zhao, Y.; Zhang, H.; Xie, S.; Li, Y. F.; Li, X.; Jiang, Z.; Liu, Z. P., Accelerated active phase transformation of NiO powered by Pt single atoms for enhanced oxygen evolution reaction. *Chem Sci* **2018,** *9* (33), 6803-6812.
[16] Pebley, A. C.; Decolvenaere, E.; Pollock, T. M.; Gordon, M. J., Oxygen evolution on Fe-doped NiO electrocatalysts deposited via microplasma. *Nanoscale* **2017,** *9* (39), 15070-15082.
[17] Han, L.; Dong, S.; Wang, E., Transition-Metal (Co, Ni, and Fe)-Based Electrocatalysts for the Water Oxidation Reaction. *Adv Mater* **2016,** *28* (42), 9266-9291.
[18] Huang, J.; Sun, Y.; Du, X.; Zhang, Y.; Wu, C.; Yan, C.; Yan, Y.; Zou, G.; Wu, W.; Lu, R.; Li, Y.; Xiong, J., Cytomembrane-Structure-Inspired Active Ni-N-O Interface for Enhanced Oxygen Evolution Reaction. *Adv Mater* **2018,** *30* (39), e1803367.
[19] Swesi, A. T.; Masud, J.; Nath, M., Nickel selenide as a high-efficiency catalyst for oxygen evolution reaction. *Energy & Environmental Science* **2016,** *9* (5), 1771-1782.
[20] Xia, B.; Wang, T.; Jiang, X.; Li, J.; Zhang, T.; Xi, P.; Gao, D.; Xue, D., N+-ion irradiation engineering towards the efficient oxygen evolution reaction on NiO nanosheet arrays. *Journal of Materials Chemistry A* **2019,** *7* (9), 4729-4733.
[21] Kumar, A.; Bhattacharyya, S., Porous NiFe-Oxide Nanocubes as Bifunctional Electrocatalysts

for Efficient Water-Splitting. *ACS Appl Mater Interfaces* **2017,** *9* (48), 41906-41915.
[22] Gu, Y.; Chen, S.; Ren, J.; Jia, Y. A.; Chen, C.; Komarneni, S.; Yang, D.; Yao, X., Electronic Structure Tuning in Ni_3FeN/r-GO Aerogel toward Bifunctional Electrocatalyst for Overall Water Splitting. *ACS Nano* **2018,** *12* (1), 245-253.
[23] Gao, Z. W.; Liu, J. Y.; Chen, X. M.; Zheng, X. L.; Mao, J.; Liu, H.; Ma, T.; Li, L.; Wang, W. C.; Du, X. W., Engineering NiO/NiFe LDH Intersection to Bypass Scaling Relationship for Oxygen Evolution Reaction via Dynamic Tridimensional Adsorption of Intermediates. *Adv Mater* **2019,** *31* (11), e1804769.
[24] Huang, C.; Ouyang, T.; Zou, Y.; Li, N.; Liu, Z.-Q., Ultrathin $NiCo_2P_x$ nanosheets strongly coupled with CNTs as efficient and robust electrocatalysts for overall water splitting. *Journal of Materials Chemistry A* **2018,** *6* (17), 7420-7427.
[25] He, J.; Wang, M.; Wang, W.; Miao, R.; Zhong, W.; Chen, S. Y.; Poges, S.; Jafari, T.; Song, W.; Liu, J.; Suib, S. L., Hierarchical Mesoporous NiO/MnO_2@PANI Core-Shell Microspheres, Highly Efficient and Stable Bifunctional Electrocatalysts for Oxygen Evolution and Reduction Reactions. *ACS Appl Mater Interfaces* **2017,** *9* (49), 42676-42687.
[26] Xu, K.; Chen, P.; Li, X.; Tong, Y.; Ding, H.; Wu, X.; Chu, W.; Peng, Z.; Wu, C.; Xie, Y., Metallic nickel nitride nanosheets realizing enhanced electrochemical water oxidation. *J Am Chem Soc* **2015,** *137* (12), 4119-25.
[27] Saddeler, S.; Bendt, G.; Salamon, S.; Haase, F. T.; Landers, J.; Timoshenko, J.; Rettenmaier, C.; Jeon, H. S.; Bergmann, A.; Wende, H.; Roldan Cuenya, B.; Schulz, S., Influence of the cobalt content in cobalt iron oxides on the electrocatalytic OER activity. *Journal of Materials Chemistry A* **2021,** *9* (45), 25381-25390.
[28] Rui, K.; Zhao, G.; Chen, Y.; Lin, Y.; Zhou, Q.; Chen, J.; Zhu, J.; Sun, W.; Huang, W.; Dou, S. X., Hybrid 2D Dual-Metal–Organic Frameworks for Enhanced Water Oxidation Catalysis. *Advanced Functional Materials* **2018,** *28* (26).
[29] Zhang, X.-Y.; Guo, B.-Y.; Lin, Z.-Y.; Dong, B.; Chen, Q.-W.; Dong, Y.-W.; Yang, M.; Wang, L.; Liu, C.-G.; Chai, Y.-M., In situ electro-reduction to modulate the surface electronic structure of Fe_3O_4 for enhancing oxygen evolution reaction. *International Journal of Hydrogen Energy* **2020,** *45* (31), 15476-15482.
[30] Liu, G.; Yao, R.; Zhao, Y.; Wang, M.; Li, N.; Li, Y.; Bo, X.; Li, J.; Zhao, C., Encapsulation of Ni/Fe_3O_4 heterostructures inside onion-like N-doped carbon nanorods enables synergistic electrocatalysis for water oxidation. *Nanoscale* **2018,** *10* (8), 3997-4003.
[31] Liang, Q.; Brocks, G.; Bieberle-Hütter, A., Oxygen evolution reaction (OER) mechanism under alkaline and acidic conditions. *Journal of Physics: Energy* **2021,** *3* (2).
[32] Ren, X.; Wu, T.; Sun, Y.; Li, Y.; Xian, G.; Liu, X.; Shen, C.; Gracia, J.; Gao, H. J.; Yang, H.; Xu, Z. J., Spin-polarized oxygen evolution reaction under magnetic field. *Nat Commun* **2021,** *12* (1), 2608.
[33] Liao, C.; Yang, B.; Zhang, N.; Liu, M.; Chen, G.; Jiang, X.; Chen, G.; Yang, J.; Liu, X.; Chan, T. S.; Lu, Y. J.; Ma, R.; Zhou, W., Constructing Conductive Interfaces between Nickel Oxide Nanocrystals and Polymer Carbon Nitride for Efficient Electrocatalytic Oxygen Evolution Reaction. *Advanced Functional Materials* **2019,** *29* (40).
[34] Khan, K.; Tareen, A. K.; Aslam, M.; Zhang, Y.; Wang, R.; Ouyang, Z.; Gou, Z.; Zhang, H., Recent advances in two-dimensional materials and their nanocomposites in sustainable energy conversion applications. *Nanoscale* **2019,** *11* (45), 21622-21678.
[35] Suen, N. T.; Hung, S. F.; Quan, Q.; Zhang, N.; Xu, Y. J.; Chen, H. M., Electrocatalysis for the oxygen

evolution reaction: recent development and future perspectives. *Chem Soc Rev* **2017,** *46* (2), 337-365.
[36] Zhong, H.; Campos-Roldán, C.; Zhao, Y.; Zhang, S.; Feng, Y.; Alonso-Vante, N., Recent Advances of Cobalt-Based Electrocatalysts for Oxygen Electrode Reactions and Hydrogen Evolution Reaction. *Catalysts* **2018,** *8* (11)

[37] Liao, C.; Yang, B.; Zhang, N.; Liu, M.; Chen, G.; Jiang, X.; Chen, G.; Yang, J.; Liu, X.; Chan, T. S.; Lu, Y. J.; Ma, R.; Zhou, W., Constructing Conductive Interfaces between Nickel Oxide Nanocrystals and Polymer Carbon Nitride for Efficient Electrocatalytic Oxygen Evolution Reaction. *Advanced Functional Materials* **2019,** *29* (40).
[38] Chang, W.; Ning, B.; Xu, Q.; Jiang, H.; Hu, Y.; Li, C., Strongly coupled N-doped graphene quantum dots/Ni(Fe)O_xH_y electrocatalysts with accelerated reaction kinetics for water oxidation. *Chemical Engineering Journal* **2022,** *430*.
[39] Wang, X. R.; Liu, J. Y.; Liu, Z. W.; Wang, W. C.; Luo, J.; Han, X. P.; Du, X. W.; Qiao, S. Z.; Yang, J., Identifying the Key Role of Pyridinic-N-Co Bonding in Synergistic Electrocatalysis for Reversible ORR/OER. *Adv Mater* **2018,** *30* (23), e1800005.
[40] Zhou, Y.; Lu, R.; Tao, X.; Qiu, Z.; Chen, G.; Yang, J.; Zhao, Y.; Feng, X.; Mullen, K., Boosting Oxygen Electrocatalytic Activity of Fe-N-C Catalysts by Phosphorus Incorporation. *J Am Chem Soc* **2023,** *145* (6), 3647-3655.
[41] Zhao, Y.; Yang, N.; Yao, H.; Liu, D.; Song, L.; Zhu, J.; Li, S.; Gu, L.; Lin, K.; Wang, D., Stereodefined Codoping of sp-N and S Atoms in Few-Layer Graphdiyne for Oxygen Evolution Reaction. *J Am Chem Soc* **2019,** *141* (18), 7240-7244.
[42] Su, H.; Zhou, W.; Zhou, W.; Li, Y.; Zheng, L.; Zhang, H.; Liu, M.; Zhang, X.; Sun, X.; Xu, Y.; Hu, F.; Zhang, J.; Hu, T.; Liu, Q.; Wei, S., In-situ spectroscopic observation of dynamic-coupling oxygen on atomically dispersed iridium electrocatalyst for acidic water oxidation. *Nat Commun* **2021,** *12* (1), 6118.
[43] Jiang, B.; Wang, T.; Cheng, Y.; Liao, F.; Wu, K.; Shao, M., Ir/g-C_3N_4/Nitrogen-Doped Graphene Nanocomposites as Bifunctional Electrocatalysts for Overall Water Splitting in Acidic Electrolytes. *ACS Appl Mater Interfaces* **2018,** *10* (45), 39161-39167.
[44] Rashid, J.; Parveen, N.; Haq, T. u.; Iqbal, A.; Talib, S. H.; Awan, S. U.; Hussain, N.; Zaheer, M., g-C_3N_4/CeO_2/Fe_3O_4 Ternary Composite as an Efficient Bifunctional Catalyst for Overall Water Splitting. *ChemCatChem* **2018,** *10* (24), 5587-5592.
[45] Nazir, R.; Fageria, P.; Basu, M.; Pande, S., Decoration of Carbon Nitride Surface with Bimetallic Nanoparticles (Ag/Pt, Ag/Pd, and Ag/Au) via Galvanic Exchange for Hydrogen Evolution Reaction. *The Journal of Physical Chemistry C* **2017,** *121* (36), 19548-19558.
[46] Zheng, Y.; Jiao, Y.; Zhu, Y.; Cai, Q.; Vasileff, A.; Li, L. H.; Han, Y.; Chen, Y.; Qiao, S. Z., Molecule-Level g-C_3N_4 Coordinated Transition Metals as a New Class of Electrocatalysts for Oxygen Electrode Reactions. *J Am Chem Soc* **2017,** *139* (9), 3336-3339.
[47] Zheng, X.; Cao, X.; Zeng, K.; Yan, J.; Sun, Z.; Rummeli, M. H.; Yang, R., A Self-Jet Vapor-Phase Growth of 3D FeNi@NCNT Clusters as Efficient Oxygen Electrocatalysts for Zinc-Air Batteries. *Small* **2021,** *17* (4), e2006183. 2.
[48] Li, Z.; Xu, X.; Lu, X.; He, C.; Huang, J.; Sun, W.; Tian, L., Synergistic coupling of $FeNi_3$ alloy with graphene carbon dots for advanced oxygen evolution reaction electrocatalysis. *J Colloid Interface Sci* **2022,** *615*, 273-281.
[49] Khan, K.; Tareen, A. K.; Aslam, M.; Zhang, Y.; Wang, R.; Ouyang, Z.; Gou, Z.; Zhang, H., Recent advances in two-dimensional materials and their nanocomposites in sustainable energy conversion

applications. *Nanoscale* **2019,** *11* (45), 21622-21678.
[50] Li, S.; Chen, B.; Wang, Y.; Ye, M. Y.; van Aken, P. A.; Cheng, C.; Thomas, A., Oxygen-evolving catalytic atoms on metal carbides. *Nat Mater* **2021,** *20* (9), 1240-1247.
[51] Tu, Y.; Ren, P.; Deng, D.; Bao, X., Structural and electronic optimization of graphene encapsulating binary metal for highly efficient water oxidation. *Nano Energy* **2018,** *52*, 494-500.
[52] Nayak, S.; Parida, K., Superactive NiFe-LDH/graphene nanocomposites as competent catalysts for water splitting reactions. *Inorganic Chemistry Frontiers* **2020,** *7* (20), 3805-3836.